

Nanoscale

Accepted Manuscript



This is an *Accepted Manuscript*, which has been through the Royal Society of Chemistry peer review process and has been accepted for publication.

Accepted Manuscripts are published online shortly after acceptance, before technical editing, formatting and proof reading. Using this free service, authors can make their results available to the community, in citable form, before we publish the edited article. We will replace this *Accepted Manuscript* with the edited and formatted *Advance Article* as soon as it is available.

You can find more information about *Accepted Manuscripts* in the [Information for Authors](#).

Please note that technical editing may introduce minor changes to the text and/or graphics, which may alter content. The journal's standard [Terms & Conditions](#) and the [Ethical guidelines](#) still apply. In no event shall the Royal Society of Chemistry be held responsible for any errors or omissions in this *Accepted Manuscript* or any consequences arising from the use of any information it contains.

Mapping plasmonic topological states at the nanoscale

Ivan S. Sinev,^a Ivan S. Mukhin,^a Alexey P. Slobozhanyuk,^{a,b} Alexander N. Poddubny,^{a,c} Andrey E. Miroshnichenko,^{*b} Anton K. Samusev,^a and Yuri S. Kivshar^b

Received Xth XXXXXXXXXXXX 20XX, Accepted Xth XXXXXXXXXXXX 20XX

First published on the web Xth XXXXXXXXXXXX 200X

DOI: 10.1039/b000000x

We report on the first experimental observation of topological edge states in zigzag chains of plasmonic nanodisks. We demonstrate that such edge states can be selectively excited with the linear polarization of the incident light, and visualize them directly by near-field scanning optical microscopy. Our work provides experimental verification of a novel paradigm for manipulating light at the nanoscale in topologically nontrivial structures.

The study of nontrivial topological properties of matter is a new and exciting area of research in condensed matter physics focusing on the realization of exotic electronic states for applications in new and advanced technologies.¹ One of the recognized topologically nontrivial phases of electronic matter is associated with the quantum Hall effect when a magnetic field applied to a two-dimensional system of free electrons breaks the time-reversal symmetry.² A similar quantum spin Hall effect relies on spin-orbit coupling³. Recently, similar concepts penetrated into the field of optics.⁴ Various suggestions are based on explicit breaking of the time-reversal symmetry by applying a periodic modulation to the structure,⁵ relatively weak magneto-optic effects,⁶ and engineering photonic crystals and metamaterials with built-in synthetic magnetic fields and spin-orbit interactions.^{7,8} The first demonstrations of *electromagnetic edge states* were achieved in the samples with the characteristic period of several centimeters operating at radio frequencies.^{9–11} Recently, the topological states of light were demonstrated at the optical frequencies in the coupled silicon waveguide arrays with the sizes of tens of microns.^{8,12–14} The waveguide-based¹⁵ and photonic crystal-based structures¹⁶ have an inherent limitation: the minimal size of their building blocks should be larger than the light wavelength. Further reduction of the structure size would allow deterministic coupling between the optical topological states and quantum excitations of the matter. This can be used for the development of optically controlled on-chip quantum computing and

communication structures robust against disorder.^{17,18}

In this Letter, we provide the first experimental verification of the existence of topological edge states realized in the sub-wavelength regime for a zigzag chain of gold nanodisks in the visible spectral range (see Fig. 1). The nontrivial topological properties of such a type of topological edge states can be illustrated in the framework of the coupled-dipole approximation.¹⁹ Below, we first recall the simplified model of Ref. 19, and then compare it with the experiment for realistic structures and discuss its limitations.

By retaining the nearest neighbour coupling only, the zigzag chain of plasmonic elements can be written in the form of two interacting sublattices,

$$\begin{aligned} \frac{1}{\alpha} \mathbf{p}_n^A &= U \mathbf{p}_n^B + V \mathbf{p}_{n-1}^B + \mathbf{E}^{(0)} \\ \frac{1}{\alpha} \mathbf{p}_n^B &= U \mathbf{p}_n^A + V \mathbf{p}_{n+1}^A + \mathbf{E}^{(0)} \end{aligned} \quad (1)$$

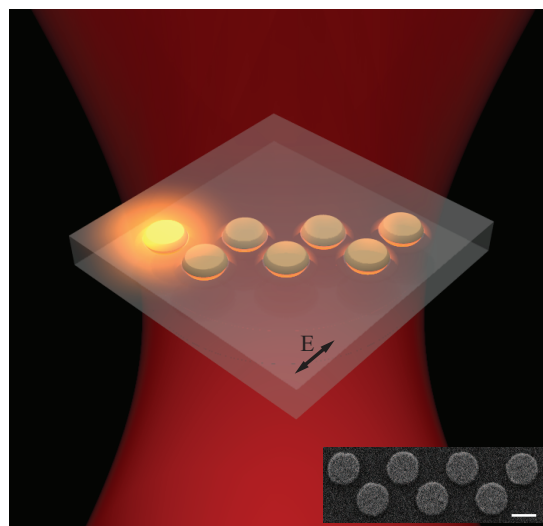


Fig. 1 Schematic illustration of an edge state in the zigzag chain of plasmonic nanodisks with odd number of nanoparticles excited by a linearly polarized light (the arrow shows the polarization direction). The inset shows the SEM image of the fabricated zigzag chain of gold nanodisks with the scale bar representing 200 nm.

* E-mail: andrey.miroshnichenko@anu.edu.au

^a ITMO University, St. Petersburg 197101, Russia

^b Nonlinear Physics Centre, Australian National University, ACT 2601, Australia

^c Ioffe Physical-Technical Institute, Russian Academy of Sciences, St. Petersburg 194021, Russia; E-mail: a.poddubny@phoi.ifmo.ru

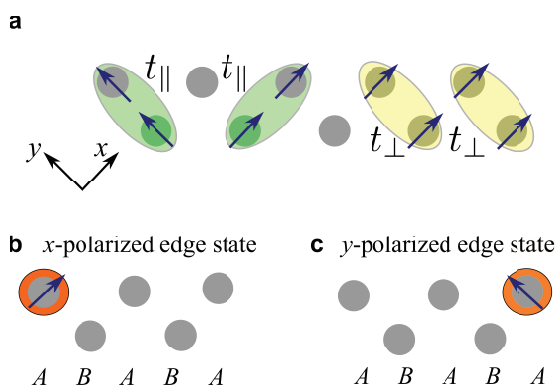


Fig. 2 Schematic illustration of (a) polarization-dependent nearest neighbor coupling between the dipole modes in the plasmonic zigzag and (b), (c) x and y -polarized edge states. The letters A and B label the two sub lattices, the arrows show the edge state polarization.

where n is the disk number, α is the in-plane dipole polarizability of the single disk, and $\mathbf{E}^{(0)}$ is the electric field of the normally incident wave, where the indices A and B stand for two sublattices. Each bond angle is formed by three consecutive disks, being equal to $\pi/2$. We consider only the plasmonic excitations polarized in the xy plane; the bonds between disks are aligned along x and y axes (see Fig. 2a). The interaction matrices U and V are diagonal and characterized by two dipole-dipole coupling constants $U_{xx} \equiv t_{\parallel} = 2/a^3$ and $U_{yy} \equiv t_{\perp} = -1/a^3$ (see Fig. 2a), where a is the distance between the adjacent disk centers. The matrix V is obtained from the matrix U by interchanging the diagonal elements, $V_{yy} = t_{\parallel}$ and $V_{xx} = t_{\perp}$.

In the nearest-neighbor approximation the x and y polarized modes in Eq. (1) are decoupled. Note here, that for each polarization the problem reduces to Su-Schrieffer-Heeger model²⁰ that has been first developed for the polyacetylene, and then applied to various dimer lattices of photons and cold atoms.^{21–24} It is known to possess nontrivial topological phases²⁵ and has been used in optics for classical simulations of Majorana dynamics.²⁶ Particularly, for each polarization there exist two bulk Bloch bands with the dispersion law $1/\alpha = \pm |t_{\parallel} + t_{\perp} e^{iK}|$, where K is the dimensionless Bloch vector. Their topologically nontrivial properties can be illustrated by means of the Zak phase

$$\Gamma_{\sigma} = -i \int_{-\pi}^{\pi} dK \langle \psi_{K,\sigma} | \partial_K | \psi_{K,\sigma} \rangle, \quad (2)$$

for the bulk Bloch excitations $\psi_{K,\sigma}$ for both bands

$$\Gamma_{\sigma} = \begin{cases} \pi, & |t_{\sigma,\text{intra}}| > |t_{\sigma,\text{inter}}| \\ 0, & \text{otherwise.} \end{cases} \quad (3)$$

Here $t_{\sigma,\text{intra}}$ and $t_{\sigma,\text{inter}}$ are the coupling constants between the disks inside the same and different unit cells, respectively. Depending on the unit cell choice and on the relation between the couplings, the Zak phase is equal to either zero or π . When the first (last) two disks of the finite chain belong to the same unit cell, i.e. the unit cell is chosen in such way that it is not broken by the edge, the non-zero value of the Zak phase means the presence of the edge mode at

$$\frac{1}{\alpha} = 0, \quad (4)$$

corresponding to the single disk resonance.

The polarization of these edge states is illustrated in Fig. 2. For odd number of disks the finite-extent chain has an x -polarized mode localized at the left edge (see Fig. 2b) and a y -polarized mode at the right one (see Fig. 2c). The x and y modes are degenerate, their frequency corresponds to the single disk resonance, Eq. (4). Such states with zero energy detuning from the resonance are the hallmark of Su-Schrieffer-Heeger model. This model also describes the origin of the Kitaev's edge states formation of in the quantum wire placed on top of a superconductor.²⁷ Hence, the spatial distribution of the Kitaev's states is very similar to the considered plasmonic edge modes. Contrary to our classical bosonic system, the Kitaev's edge states for the quantum wire have the statistics of Majorana fermions. There have been a number of proposals to mimic the Majorana fermions in optical systems.^{26,28,29} Our system could probably be used for that only in the strongly nonlinear quantum regime of fermionized photons.³⁰ However, its essential feature, revealed already in the considered classical regime, is the possibility to resonantly excite either left or right edge of the zigzag chain with odd number of nanodisks simply by switching the corresponding linear polarization direction of the incident plane wave \mathbf{E}_0 . For even number of disks the structure supports simultaneously both edge states, which are in this case co-polarized and excited with the same amplitude.

In order to demonstrate the effect experimentally, we have fabricated a zigzag chain of seven gold nanodisks on a glass substrate using the electron beam lithography. The disks had a diameter of 250 nm and a height of approximately 40 nm, while the distance between adjacent disk edges was equal to 100 nm (see the scanning electron microscopy (SEM) image in the inset of Fig. 1). The electron exposure was carried out on the 120 nm PMMA layer covered with thin 10 nm Au layer for charge draining. After the gold layer was removed and the exposed electron resist was developed, the Cr/Au layers were thermally evaporated with 3 nm and 40 nm thicknesses, respectively and the procedure was finalized with lift-off.

The structure is illuminated from the substrate side by a weakly focused linearly polarized laser beam as it is sketched in Fig. 1. The central wavelength of the excitation was con-

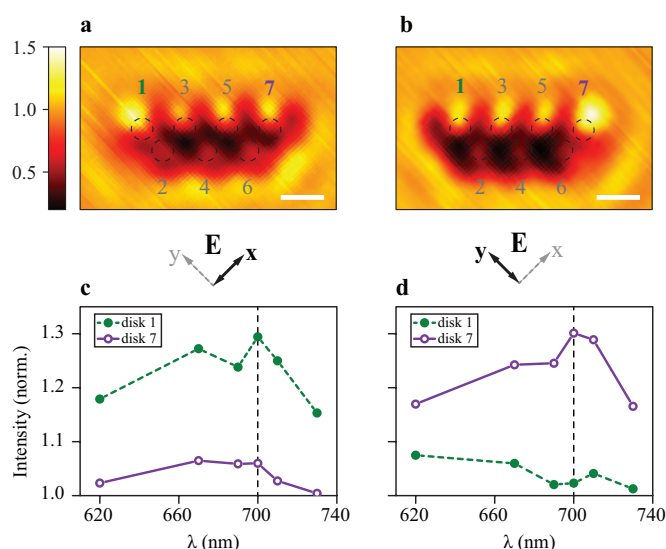


Fig. 3 Experimental observation of topological edge states at the nanoscale. **a,b**, Near-field patterns of the polarization-sensitive localized plasmonic modes measured at the 100 nm distance from the substrate surface for 700 nm excitation wavelength for x - (**a**) and y - (**b**) polarizations. The scale bars represent 500 nm. **c,d**, Spectral dependence of the normalized intensity of the hot spots corresponding to the 1-st and 7-th disks for x - (**c**) and y - (**d**) polarizations of the incident wave.

tinuously tuned around the resonance of the individual disk, and the near-field patterns of the plasmonic modes induced in the structure were measured by an aperture-type near-field scanning optical microscope (NSOM, AIST-NT) in the collection mode. In order to tune the excitation wavelength within all the visible spectral range, we employed a supercontinuum source (Fianium WhiteLase SC400-6) combined with the tunable filter (Fianium SuperChromeTM) yielding a beam with the spectral width of approximately 10 nm. After the filtering, the beam was polarized with a Glan-Taylor prism and weakly focused on the sample surface by a achromatic doublet lens (focal distance $f = 5$ cm) to a spot with the diameter of approximately $15 \mu\text{m}$. The near-field signal was collected with tapered aluminium-coated fiber probe with an aperture diameter of approximately 150 nm. The scanning process was performed in constant-height mode (height $h = 100$ nm above the substrate surface) by using capacitive sensor feedback loop. Due to relatively fast scanning rate, the drifting between the probe and the sample while measuring a single near-field map was negligible.

Fig. 3 presents our main results: map of the near field at the $\lambda = 700$ nm wavelength. As predicted by the analytical model, the distribution exhibits hot spots at the edges of the structure, which is the signature of the excitation of different edges of the structure depending on the polarization. The positions of

the spots are slightly shifted from the disk centers, which are denoted by the respective digits (see Supplementary Fig. S2 for the exact positions of the disks). We associate this effect with strong probe-sample interaction. The resonant plasmonic structures appearing dark in the near-field maps were also reported in works by Denkova *et al.* and Okamoto *et al.*^{31,32}

By switching between two orthogonal polarizations of the incident wave, we can excite either the left edge [disk #1 in Fig. 3a] or the right edge [disk #7 in Fig. 3b] of the chain in agreement with Fig. 2. The effect also has clear resonant behavior, which is illustrated in Figs. 3(c,d). The lines show spectral dependence of the signal obtained from the disks #1 and #7 normalized to the average signal from the two central disks (#3 and #5) in the top row of the chain for two respective polarizations. The absolute intensity for each disk was obtained by integrating the near-field signal over the bright spot corresponding to the respective disk. The pronounced spectral maxima for the disks #1 and #7 in the x and y polarizations, respectively, are in agreement with the analytical prediction of the edge state excitation at the condition Eq. (4). The NSOM maps for all presented wavelengths can be found in Supplementary.

To analyze the experimental results in more detail we perform the full-wave numerical simulation, summarized in Fig. 4. The calculations were performed using the frequency domain solver of the CST Microwave Studio[®] 2014 software. The zigzag chain was excited by a linearly polarized plane wave.

Panel (a) in Fig. 4 presents the calculated absorption and scattering cross sections for a zigzag structure in free space. The scattering spectrum is dominated by the dipole resonance peak at the wavelength $\lambda \approx 700$ nm, which is strongly broadened due to the radiative losses. At the same time, the absorption spectrum has also a sharp resonant feature at the wavelength $\lambda \approx 600$ nm, corresponding to the quadrupole resonance. This is the resonance of the double-degenerate over polarization ($x^2 - y^2$ and $2xy$) quadrupole mode, that is not directly excited for a single disk at normal light incidence. This quadrupole mode becomes optically active due to the symmetry reduction in the zigzag chain (see Supplementary Information for more details). While the quadrupole resonance is not resolved in the far-field scattering spectra, it is quite important in the near-field excitation.

In the NSOM experiment, however, the optical properties of the chain are significantly influenced by the substrate and the near-field probe. To account for these factors in the simulations, the CST model was extended by adding the substrate with a refractive index of 1.5, while the presence of the near-field probe was modelled by a perfectly conducting (PEC) layer placed at a distance of 100 nm from the substrate (see the Supplementary for more details). The maps of magnetic and electric components of the near field of the structure under the

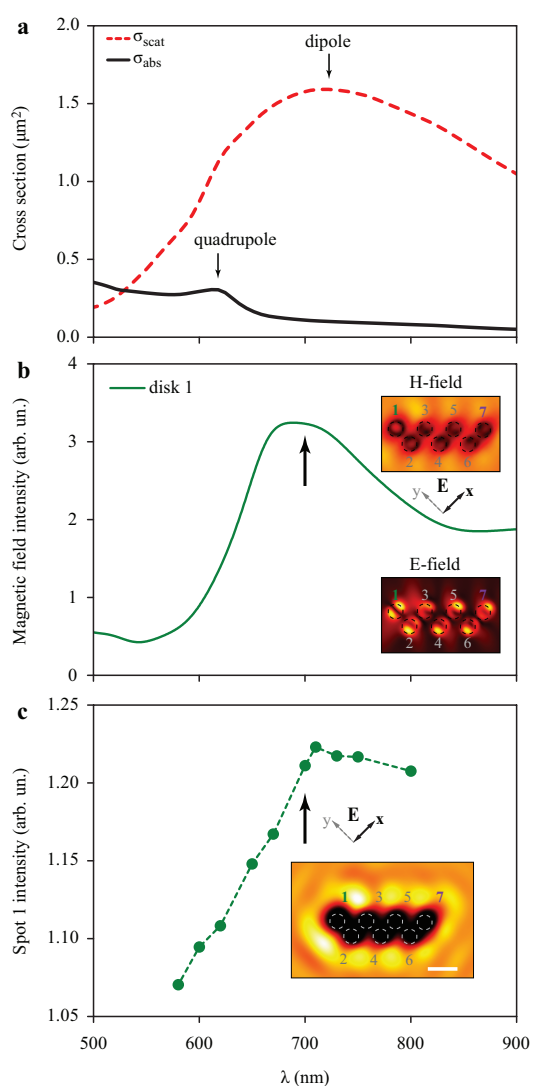


Fig. 4 Numerical simulations of gold nanodisks zigzag. (a) Calculated absorption (σ_{abs}) and scattering (σ_{scat}) cross sections of the 7-disk structure, under y -polarized excitation in free space. Vertical arrows show the positions of the dipole- and quadrupole-like resonances. (b) Spectral dependence of the normalized magnetic field intensity at 50 nm above the center of disk #1, illustrating the excitation of the edge state. The insets show the two-dimensional maps of the amplitudes of magnetic and electric near fields at a distance of 50 nm above the disks. (c) Spectral dependence of the relative intensity of the hot spot corresponding to the disk #1 in the numerically reconstructed near-field signal maps. The inset shows the two-dimensional map of the reconstructed near-field signal at a wavelength of 700 nm with the scale bar representing 500 nm.

PEC layer for $\lambda = 700$ nm are shown in the inset of Fig. 4b. The green curve in the main part of Fig. 4b shows the magnetic field intensity 50 nm above the center of disk #1 normalized to the mean magnetic field intensity above disks #3 and #5. This indicates that the most clear way to demonstrate the edge state would be to directly measure the near magnetic field, where the edge state is manifested by a resonantly excited hot spot above one of the edge disks.

The actual signal collected by the near-field probe, however, can depend on both electric and magnetic fields³³ as well as on the probe shape and permittivity, and it is also influenced by the probe-sample interaction which can be strong in the case of plasmonic structures.³¹ In order to reconstruct the measured near-field signal, we perform the rigorous procedure based on the convolution of the calculated fields with the probe response function (see Supplementary for a detailed derivation based on the reciprocity theorem).³⁴ The reconstructed near-field map for the wavelength $\lambda = 700$ nm is shown in the inset of Fig. 4c. The comparison with experimental near-field maps does not show one-to-one correspondence (side-by-side comparison between all experimental and reconstructed near-field signal maps can be found in Supplementary Fig. S2), with bright spots shifted in different directions with respect to the disks positions. This inconsistency can be explained by the inaccuracies of the probe model we use, which does not account for the size of a real probe, its specific shape and other complex interactions, such as excitation of surface plasmon polariton on the probe coating, multiple scattering, etc., which are too difficult to be fully included in the simulation.

However, a careful analysis of the spectral dependence of the intensities of bright spots observed in experimental and numerically reconstructed near-field maps proves that in both cases they characterize the edge state excitation. The curve in Fig. 4c shows the spectral dependence of the signal obtained from the disk #1 normalized to the average signal from the two central disks (#3 and #5) for x -polarization. In exactly the same way as for the experimental curves in Fig. 3c,d, the absolute intensity for each disk is obtained by integrating the near-field signal over the bright spot corresponding to the respective disk. Both experimental (Fig. 3c,d) and numerical (Fig. 4c) curves closely follow the spectral dependence of the magnetic field localization shown in Fig. 4b, confirming that bright spots in the experimental and numerically reconstructed near-field maps indeed characterize the excitation of the edge state in the zigzag chain.

The comparison of the scattering and absorption spectra (Fig. 4a) with experimental (Fig. 3c,d) and numerical (Fig. 4b,c) near field spectra unambiguously supports our attribution of the resonantly excited edge states to the dipole resonance of individual disks, with possible admixture of the quadrupole mode. The coupled-dipoles model associated with the Su-Schrieffer-Heeger model, Eq. (1), does not take all

the features of the actual sample into account. The particular simplifications include neglected Ohmic and radiation losses, long-range interaction,³⁵ and quadrupole modes. Nevertheless, the main model prediction, the frequency-selective polarization-controlled excitation of the edge modes, turns out to be quite robust.

To summarize, we have visualized nanoscale topological edge states of plasmons by means of the near-field scanning optical microscopy. The studied nanostructure, a zigzag chain of plasmonic nanodisks, presents a classical counterpart of the Kitaev's model for the Majorana fermions in the quantum wire above the superconductor. We have exploited the polarization degree of freedom of light to realize a resonant selective excitation of the edge disks. This uncovers the potential of the plasmonic disk chains for a variety of compact nanodevices such as polarization-tunable nanoantennas and light sensors; and even richer physics can be sought for in the nonlinear and/or few-photon regimes.

Acknowledgement

We thank A. Khanikaev and I. Shadrivov for useful comments and suggestions. The work of I.S.S., I.S.M., A.N.P., and A.K.S. was supported by Ministry of Education and Science of the Russian Federation (projects GOSZADANIE 2014/190, Zadanie No. 3.561.2014/K, No. 3.1231.2014/K, and project 14.584.21.0009 10) and the Russian Foundation for Basic Research. ANP acknowledges the support of the RF President Grant No. MK-6029.2014.2. The work of AEM was supported by the Australian Research Council.

References

- B. A. Bernevig, T. L. Hughes and S.-C. Zhang, *Science*, 2006, **314**, 1757–1761.
- D. J. Thouless, M. Kohmoto, M. P. Nightingale and M. den Nijs, *Phys. Rev. Lett.*, 1982, **49**, 405–408.
- C. L. Kane and E. J. Mele, *Phys. Rev. Lett.*, 2005, **95**, 146802.
- L. Lu, J. D. Joannopoulos and M. Soljacic, *Nat Photon*, 2014, **8**, 821–829.
- K. Fang, Z. Yu and S. Fan, *Nature Photonics*, 2012, **6**, 782–787.
- F. D. M. Haldane and S. Raghu, *Phys. Rev. Lett.*, 2008, **100**, 013904.
- A. B. Khanikaev, S. Hossein Mousavi, W.-K. Tse, M. Kargarian, A. H. MacDonald and G. Shvets, *Nature Materials*, 2013, **12**, 233–239.
- M. C. Rechtsman, J. M. Zeuner, Y. Plotnik, Y. Lumer, D. Podolsky, F. Dreisow, S. Nolte, M. Segev and A. Szameit, *Nature*, 2013, **496**, 196–200.
- Z. Wang, Y. Chong, J. D. Joannopoulos and M. Soljačić, *Nature*, 2009, **461**, 772–775.
- W. Tan, Y. Sun, H. Chen and S.-Q. Shen, *Scientific Reports*, 2014, **4**, 3842.
- W.-J. Chen, S.-J. Jiang, X.-D. Chen, B. Zhu, L. Zhou, J.-W. Dong and C. T. Chan, *Nat Commun*, 2014, **5**, 5782.
- Y. E. Kraus and O. Zilberberg, *Phys. Rev. Lett.*, 2012, **109**, 116404.
- M. Verbin, O. Zilberberg, Y. E. Kraus, Y. Lahini and Y. Silberberg, *Phys. Rev. Lett.*, 2013, **110**, 076403.
- M. Hafezi, S. Mittal, J. Fan, A. Migdall and J. M. Taylor, *Nature Photonics*, 2013, **7**, 1001.
- T. Ma, A. B. Khanikaev, S. H. Mousavi and G. Shvets, *ArXiv e-print*, 2014.
- T. Jacqmin, I. Carusotto, I. Sagnes, M. Abbarchi, D. Solnyshkov, G. Malpuech, E. Galopin, A. Lemaître, J. Bloch and A. Amo, *Phys. Rev. Lett.*, 2014, **112**, 116402.
- M. Hafezi, E. A. Demler, M. D. Lukin and J. M. Taylor, *Nature Physics*, 2011, **7**, 907–912.
- T. C. H. Liew and V. Savona, *New Journal of Physics*, 2013, **15**, 025015.
- A. Poddubny, A. Miroshnichenko, A. Slobozhanyuk and Y. Kivshar, *ACS Photonics*, 2014, **1**, 101–105.
- A. J. Heeger, S. Kivelson, J. R. Schrieffer and W. P. Su, *Rev. Mod. Phys.*, 1988, **60**, 781–850.
- I. L. Garanovich, A. A. Sukhorukov and Y. S. Kivshar, *Phys. Rev. Lett.*, 2008, **100**, 203904.
- H. Schomerus, *Opt. Lett.*, 2013, **38**, 1912–1914.
- X. Li, E. Zhao and W. Vincent Liu, *Nature Communications*, 2013, **4**, 1523.
- M. Atala, M. Aidelsburger, J. T. Barreiro, D. Abanin, T. Kitagawa, E. Demler and I. Bloch, *Nature Physics*, 2013, **9**, 795–800.
- S.-Q. Shen, *Topological Insulators. Dirac Equation in Condensed Matter*, Springer, Heidelberg, 2013.
- R. Keil, C. Noh, A. Rai, S. Stützer, S. Nolte, D. G. Angelakis and A. Szameit, *ArXiv e-prints*, 2014.
- A. Y. Kitaev, *Physics-Uspekhi*, 2001, **44**, 131.
- B. M. Rodríguez-Lara and H. M. Moya-Cessa, *Phys. Rev. A*, 2014, 015803.
- C. Noh, B. M. Rodríguez-Lara and D. G. Angelakis, *Phys. Rev. A*, 2013, **87**, 040102.
- I. Carusotto, D. Gerace, H. E. Tureci, S. De Liberato, C. Ciuti and A. Imamoglu, *Phys. Rev. Lett.*, 2009, **103**, 033601.
- D. Denkova, N. Verellen, A. V. Silhanek, P. Van Dorpe and V. V. Moshchalkov, *Small*, 2014, **10**, 1959–1966.
- H. Okamoto and K. Imura, *The Journal of Physical Chemistry Letters*, 2013, **4**, 2230–2241.
- B. le Feber, N. M. Rotenberg, D. Beggs and L. Kuipers, *Nat Photon*, 2014, **8**, 43–46.
- J. Porto, R. Carminati and J.-J. Greffet, *Journal of Applied Physics*, 2000, **88**, 4845–4850.
- A. Poshakinskiy, A. Poddubny, L. Pillozzi and E. Ivchenko, *Phys. Rev. Lett.*, 2014, **112**, 107403.